An Estimation of Sea-Level and Surface-Current Anomalies during the 1972 El Niño and Consequent Thermal Effects

A. E. GILL

Department of Applied Mathematics and Theoretical Physics, University of Cambridge, Silver Street, Cambridge CB39EW, England

(Manuscript received 6 July 1982, in final form 30 November 1982)

ABSTRACT

This paper has two main parts. First, it is shown that if the dynamics is simplified by assuming a one-mode, low-frequency (or long-wave) model, the whole field of anomalous motion in the tropical region can be deduced from the time series of sea-level anomaly at the eastern boundary. This is because the amplitudes of all the equatorial waves are proportional to sea level at this longitude, and the amplitudes at other longitudes can be deduced by integrating along characteristics using the method of Gill and Clarke (1974). The integration proceeds forward in time for the planetary waves and backward in time for the Kelvin wave. The calculation requires a knowledge of wind stress anomalies, although the wind effect only becomes significant after integration to large distances from the eastern boundary. The western boundary is irrelevant to the calculations. The technique is applied to estimate zonal surface current anomalies in the equatorial Pacific for the period 1971–73 spanning a major El Niño. Mean zonal surface current anomalies within ±5° of the equator are deduced to have reached their largest values (of ~0.5 m s^{-1}) near the date line in early 1972, when they were eastward, and in early 1973, when they were westward.

The second part of the paper uses the reconstructed anomaly field of the first part to examine anomalies in the heat balance of the surface layer of the equatorial Pacific. The striking result here is that surface temperature anomalies in the central Pacific are well reproduced in both amplitude and timing if caused solely by horizontal advection by the zonal current anomaly. Other mechanisms give much smaller amplitude and the wrong timing. The resultant picture is that warm anomalies in the central Pacific result from huge anomalous eastward movements of warm water from the west Pacific.

The heat balance near the eastern boundary is also discussed, and two possible mechanisms seem capable of reproducing a warm anomaly with the correct strength at the right time. One is anomalous poleward advection of warm water along the coast. The other is upwelling of anomalously warm water near the coast and the spreading of this warm anomaly by advection with the mean flow.

1. Introduction

This paper is on changes in the ocean associated with the El Niño/Southern Oscillation. In particular, a method is described for estimating anomalies in surface currents, and calculations are made for changes associated with the 1972 event. The dramatic changes in surface temperature and surface winds that occur in the equatorial Pacific during these events are well known and have been documented by many authors [see Rasmusson and Carpenter (1982)]. Changes in subsurface thermal structure associated with the 1972 event have been described by Gill (1982b). However, little is known about the corresponding changes in ocean currents because few direct measurements of currents are available. Yet it is important to know these changes in order to estimate advective effects on the thermal field. In this paper a method of reconstructing the surface current field is developed. The results indicate that horizontal advection by anomalous zonal currents is the primary cause of the surface temperature anomalies on the equator in the central Pacific.

The discussion of thermal effects will be left until Section 7 and subsequent sections. For now, we consider the problem of estimating changes in currents and sea level. One approach, which has been used with some success by Busalacchi and O'Brien (1981), is to calculate the response of the ocean to observed wind stress changes using a numerical model. In particular, they found that the pycnocline height anomaly at the eastern boundary of their model correlated well with the observed sea-level anomaly at the Galapagos Islands for the ten-year period of integration (the 1960's). The correlation coefficient was 0.44, significant at the 99% level, despite deficiencies in the quality of the wind date and the simplicity of the model dynamics.

The idea that changes in the wind stress in the west Pacific can cause sea-level variations on the eastern boundary comes from observations (Hickey, 1975; Wyrtki, 1975). The effect is easily reproduced in sim-

ple reduced gravity or single mode models as shown with idealized wind stress distributions by many investigators (e.g., Hurlburt *et al.*, 1976; McCreary, 1976; Cane, 1979); Busalacchi and O'Brien (1981) showed that the linear version of such a model has skill in predicting sea-level variations using observed wind variations.

Encouraged by this success, a model with virtually the same dynamics is used in this paper, but the method of deducing the response is completely different. Before discussing the new technique, consider the nature of the dynamical assumptions that are made in order to get the simplest possible system which, despite its simplicity, has some skill in reproducing observed behavior. First, it is assumed that anomalies can be treated as small perturbations from a state of rest, although it is known (see, e.g., Gill, 1982b) that changes in some places, at least, are so large that nonlinear effects are not likely to be negligible. This assumption of linearity has the advantage that the perturbations can be expressed as a sum of vertical normal modes (Gill and Clarke, 1974; Gill, 1982a, Section 6.11). It is further assumed that the major contribution to sea-level changes and surface currents is produced by the first baroclinic mode so that the other modes can be neglected. Evidence in support of this for a different frequency range is given by Wunsch and Gill (1976). For the low frequencies of interest, subsurface data supports the idea that the first mode gives the dominant contribution in the central Pacific (Gill, 1982b) although the same is not true near the eastern boundary where the second mode fits the data better. No account is taken of this in the present calculation, nor in the other one-mode or reduced gravity models.

The equations for a single baroclinic mode are the same as those for a linear reduced gravity model in which there is one active layer over a resting deep layer. The only parameter which affects the calculation is the wave speed c that a disturbance has in the absence of rotation. Here the value 2.8 m s^{-1} is used whereas Busalacchi and O'Brien (1981) used 2.45 m s^{-1}. There is also a difference of interpretation when it comes to giving a magnitude to surface currents, as the reduced gravity model just gives the averaged current over the upper active layer. Here the surface current is evaluated on the basis of the first-mode interpretation. One further simplification used in this paper is the "low frequency" or "long wave" approximation which seems well justified because the time scale of interest is so much larger than the basic time scale of equatorial waves, which is approximately one day (Gill and Clarke, 1974; Gill, 1975; Gill, 1982a). A consequence of this assumption is that low-frequency changes in sea-level at the Galapagos Islands and the South American coast should be the same. The changes are, in fact, highly correlated (Wyrtki, 1975) but are not exactly the same.

On completing discussion of the assumptions of the model, we now investigate the model behavior when wind forcing is imposed. The response can be described in terms of equatorial trapped waves (see Gill, 1982a), which consist of one eastward traveling Kelvin wave and an infinite set of westward-traveling planetary waves. Certain reflection conditions are satisfied at the eastern and western boundaries. The response of any point in the ocean is found by summing the contributions from all the waves. The contribution from any one wave can be found using the method of characteristics outlined by Gill and Clarke (1974). This method is simple to apply as each wave travels at constant speed to the east or west. The wave contribution at a particular longitude is found by integrating *backwards* in time along a characteristic, calculating the appropriate wind effect at each point on the characteristic. This is straightforward until the characteristic meets the eastern or western boundary, where reflection conditions need to be applied, and these involve all the waves. The accuracy of the calculation depends on the accuracy of the reflection conditions, which may not be good in a complicated region like the west Pacific.

The present technique avoids the problem of the western boundary by using additional information derived from observation, namely the sea-level at the eastern boundary. For convenience, this boundary is assumed to be meridional. The boundary condition here is such that the amplitudes of *all* the waves are proportional to the sea-level anomaly and so can be calculated explicitly. Thus, the planetary waves contribution at a particular longitude can be found by integrating back along the characteristic to the eastern boundary where the known amplitude is used to give the complete solution. Similarly, the Kelvin wave contribution can be found by integrating *forward* in time to the eastern boundary. This can be done because it is a *hindcasting* problem that is being undertaken, and winds and sea-levels subsequent to an event of interest are known in addition to those preceding the event. It turns out that, for much of the equatorial Pacific, the dominant contribution to *anomalies* in surface current and sea-level comes from the sea-level anomaly input into the calculation and not from the wind anomaly input. Hence the calculation is very different from that of Busalacchi and O'Brien (1981), where the anomalies are determined entirely by contributions from wind anomalies at previous times.

The arrangement of the remainder of the paper is as follows. The reconstruction of the sea-level anomaly and surface current anomaly field is presented in Sections 2 to 6. The model and the relevant equations are established in Sections 2 and 3, and the method of reconstruction when wind corrections are ignored is established in Section 4. Wind corrections are discussed in Section 5. In Section 6 results are compared

with sea-level data for islands in the central Pacific and the comparison for the years 1971 and 1972 is made. Also, a very simple approximation is given for a quick estimation of central Pacific sea-level anomaly from the eastern boundary sea-level anomaly.

Sections 7 and 8 state the causes of thermal anomalies, first with the central Pacific, and then with the east Pacific. Section 9 describes the balance for an equatorial strip running from the date line to the American coast. In Section 7, the temperature anomaly due to surface heating is compared with that due to horizontal advection, and only the latter is found to match observations. The cause of anomalies near the eastern boundary is discussed in Section 8. Finally, a consistent picture for the heat balance in an equatorial strip is developed in Section 9. There is also a discussion (Section 10) where the following question is asked: "How much of the Kelvin wave amplitude as observed at the eastern boundary is simply carried through from the western boundary by wave propagation, and how much is due to build-up by wind input as the wave progresses across the ocean?" The data used for this study indicates the former contribution to the amplitude (which is deduced as a residual) is the larger.

2. The equations for long baroclinic waves

For small perturbations to a stratified resting ocean, the solution may be expressed as the sum of normal modes, each of which satisfies a form of the shallow-water equations (Gill, 1982a). Here attention is restricted to the first baroclinic mode only. The shallow-water equations for this mode may, assuming the beta-plane and Boussinesq approximations are appropriate, be written as

$$\frac{\partial u}{\partial t} - \beta y v = -g\frac{\partial \eta}{\partial x} + \frac{B\tau^x}{\rho}, \tag{2.1}$$

$$\frac{\partial v}{\partial t} + \beta y u = -g\frac{\partial \eta}{\partial y} + \frac{B\tau^y}{\rho}, \tag{2.2}$$

$$\frac{\partial \eta}{\partial t} + H_e\left(\frac{\partial u}{\partial x} + \frac{\partial v}{\partial y}\right) = 0, \tag{2.3}$$

where (x, y) represents distances eastwards and northwards, respectively, from the point where the equator crosses the eastern boundary, (u, v) are the corresponding velocity components, (τ^x, τ^y) the corresponding surface stress components, η is the surface elevation, ρ the density, g the acceleration due to gravity and β is the gradient of the Coriolis parameter at the equator. The two quantities which are specific to the particular mode are the equivalent depth H_e and the "equivalent forcing depth" (see Gill, 1982a) B^{-1}. The depth H_e is related to wave speed c that a disturbance would have in the absence of rotation by

$$gH_e = c^2. \tag{2.4}$$

In the central equatorial Pacific, c has a value (Wunsch and Gill, 1976), of ~ 2.7 m s^{-1} corresponding to an equivalent depth of 73 cm. The value of B is estimated by Wunsch and Gill (1976) to be about

$$B = 3.5 \times 10^{-3} \text{ m}^{-1}. \tag{2.5}$$

The value was estimated, assuming that the stress is applied as a body force over an upper mixed layer, and is found not to be very sensitive to the precise choice of mixed-layer depth (Wunsch and Gill, 1976).

Since only one mode is being considered, the vector (u, v) in (2.1)–(2.3) may conveniently be defined as the surface current and hence as the current throughout the mixed layer. Also η can be defined as the surface elevation so that (2.1) and (2.2) have their usual meaning as the horizontal momentum equations applied at the surface. Values of the current and of the perturbation pressure at other levels could be inferred from the known variations with depth of these quantities for the first baroclinic mode. However, only the surface values are considered in this paper.

Following Gill (1975) and Gill and Clarke (1974), the equations can be put in non-dimensional form by choosing as the unit of horizontal distance the equatorial Rossby radius a_e given by

$$a_e = (c/2\beta)^{1/2}, \tag{2.6}$$

and as unit of time

$$T_e = (2\beta c)^{-1/2}. \tag{2.7}$$

The value of a_e is ~ 240 km or 2.2 deg latitude, whereas the value of T_e is ~ 1.0 days. In these units, the wave speed is unity.

For the dependent variables, the unit of surface elevation can be taken as the equivalent depth and the unit of horizontal velocity as the wave speed. For linear theory to be strictly valid, values in these units should be small. The non-dimensional stress (X, Y) is defined by

$$(X, Y) = \rho^{-1}B(2\beta c^3)^{-1/2}(\tau^x, \tau^y). \tag{2.8}$$

This is equivalent to having a stress scale of 8.6 N m^{-2} (86 dyn cm^{-2}). Another way of expressing stress is in units of m^2 s^{-2} at anemometer height. Assuming a drag coefficient of 0.0015, the corresponding unit of stress is 4800 m^2 s^{-2}.

In practice, the time scales of interest are much larger than T_e as witnessed by the fact that only monthly mean data values are used for the calculations. Also, the east–west scale is much larger than a_e. These facts are the basis of the low-frequency or long-wave approximation which is discussed by Gill and Clarke (1974) and by Cane and Sarachik (1981). The effect of this approximation is to eliminate the meridional acceleration and the wind-stress term in (2.2) so that the non-dimensional equations become

$$\frac{\partial u}{\partial t} - \tfrac{1}{2}yv = -\frac{\partial \eta}{\partial x} + X, \tag{2.9}$$

$$\tfrac{1}{2}yu = -\frac{\partial \eta}{\partial y}, \tag{2.10}$$

$$\frac{\partial \eta}{\partial t} + \frac{\partial u}{\partial x} + \frac{\partial v}{\partial y} = 0. \tag{2.11}$$

The potential vorticity equation may be derived by adding the y-derivative of (2.9) to $\frac{1}{2}y$ multiplied with (2.11) and subtracting the x-derivative of (2.10). The result is

$$\frac{\partial}{\partial t}\left(\frac{\partial u}{\partial y} + \tfrac{1}{2}y\eta\right) - \tfrac{1}{2}v = \frac{\partial X}{\partial y}. \tag{2.12}$$

This gives a useful relationship at the eastern boundary, $x = 0$, which will be assumed to be meridional. Since

$$u = 0 \quad \text{at} \quad x = 0, \tag{2.13}$$

(2.10) implies that

$$\eta = \eta_E(t) \quad \text{at} \quad x = 0, \tag{2.14}$$

i.e., the surface elevation has the same value η_E at all points on the eastern boundary at any given time. Then (2.12) gives the value of the alongshore velocity v on this boundary by

$$v = y\frac{d\eta_E}{dt} + 2\frac{\partial X}{\partial y} \quad \text{at} \quad x = 0. \tag{2.15}$$

3. Separation into Kelvin waves and planetary waves

In order to express the solution of (2.9), (2.10) and (2.11) in terms of planetary waves, it is advantageous (Gill and Clarke, 1974; Gill, 1975) to replace u and η as dependent variables by their sum and difference, and then to expand the new variables in parabolic cylinder functions $D_n(y)$ (Erdelyi *et al.*, 1953; Abramowitz and Stegun, 1964), i.e.,

$$\left.\begin{aligned} q \equiv \eta + u &= \sum_{n=0}^{\infty} q_n(x, t)D_n(y) \\ r \equiv \eta - u &= \sum_{n=0}^{\infty} r_n(x, t)D_n(y) \end{aligned}\right\}, \tag{3.1}$$

and similarly for v and X. The first few functions D_n are given by

$$D_n(y) = \exp(-\tfrac{1}{4}y^2)\{1; y; y^2 - 1; y^3 - 3y\}, \quad n = 0, 1, 2, 3, \tag{3.2}$$

with higher order functions given by the recurrence relation

$$D_{n+1} = yD_n - nD_{n-1}. \tag{3.3}$$

The resulting equations (see Gill and Clarke, 1974) are first,

$$\frac{\partial q_0}{\partial t} + \frac{\partial q_0}{\partial x} = X_0. \tag{3.4}$$

This represents the Kelvin wave which, in the absence of forcing, propagates eastwards at unit speed. Second,

$$q_1 = 0, \quad v_0 = -X, \tag{3.5}$$

which is the long-wave approximation to the mixed planetary–gravity wave. Finally, the planetary wave equations are ($n = 1, 2, 3 \cdots$)

$$(2n + 1)\frac{\partial q_{n+1}}{\partial t} - \frac{\partial q_{n+1}}{\partial x} = P_{n+1} \equiv nX_{n+1} - X_{n-1}, \tag{3.6}$$

$$r_{n-1} = (n + 1)q_{n+1}, \tag{3.7}$$

$$v_n = (n + 1)\left(2\frac{\partial q_{n+1}}{\partial t} - X_{n+1}\right) + X_{n-1}. \tag{3.8}$$

In the absence of forcing, these waves propagate westward at speed $(2n + 1)^{-1}$. The forcing functions $X_n(x, t)$ can be found using the orthogonality condition

$$\int_{-\infty}^{\infty} D_nD_m dy = n!(2\pi)^{1/2}\delta_{nm}, \tag{3.9}$$

e.g., for a latitude independent wind, this gives

$$X_0 = \sqrt{2}X, \quad X_2 = \tfrac{1}{2}X_0, \quad X_4 = \tfrac{1}{4}X_2 \cdots \tag{3.10}$$

if X constant.

For realistic winds, X_0 nearly always has the same sign that X has at the equator, so a westerly wind ($X > 0$) tends to build up a Kelvin wave with positive surface elevation. Note also that, in the steady state, (3.4) shows that the surface slopes up to the east when X_0 is positive.

4. The reflection condition and the free wave solution

The boundary condition at the eastern boundary $x = 0$ is given by (2.13), which implies (2.14), and hence by (3.1) that

$$q = r = \eta_E(t) \quad \text{at} \quad x = 0. \tag{4.1}$$

Using the orthogonality condition (3.9), it follows in the same way as (3.10) that the functions q_n satisfy

$$q_0 = \sqrt{2}\eta_E, \quad q_2 = \tfrac{1}{2}q_0, \quad q_4 = \tfrac{1}{4}q_2 \cdots \quad \text{at} \quad x = 0, \tag{4.2}$$

and

$$q_1 = q_3 = q_5 = \cdots = 0 \quad \text{at} \quad x = 0. \tag{4.3}$$

Similar conditions apply to the r_n and it is easily confirmed that this is consistent with (3.7).

The significance of (4.2) and (4.3) is that all the q_n, and hence all the wave amplitudes, are given in terms of a *single function* $\eta_E(t)$ at the eastern boundary. Furthermore η_E is *known from observations* as the sea-level at the eastern boundary, or rather, as the

sea-level *anomaly* at the eastern boundary since the theory is applied only to the anomaly in this paper. In practice, the long-wave theory cannot be expected to apply too far from the equator, so sea-level anomaly at Talara (5°S), or La Libertad (2°S), might be chosen to give η_E. Alternatively, the value at Baltra (½°S, 90°W), Galapagos Islands, should be quite close to η_E and is the value used in this paper. The sea-levels at these three points behave quite similarly (Wyrtki, 1975) but are not exactly the same, the differences giving a measure of the errors involved in using long-wave theory.

Now consider a case where there is no wind anomaly in the eastern part of the ocean, i.e., the forcing terms are all zero. Then the equations of the last section have their free-wave solutions in this region. The unforced solution of (3.4) for the Kelvin wave is simply

$$q_0 = \sqrt{2}\eta_E(t - x), \tag{4.4}$$

and the solution of (3.6) for the planetary waves is simply

$$(n + 1)(n - 1)\cdot\cdot\cdot 1 \cdot q_{n+1} = \sqrt{2}\eta_E[t + (2n + 1)x], \tag{4.5}$$

for n odd (symmetric waves). The asymmetric planetary waves are zero by (4.3). Thus the long-wave solution for the entire domain is now known. The r_{n-1} and v_n follow from (3.7) and (3.8), the series of the form (3.1) can be added to give q, r and v, and finally u and η follow from (3.1). Note that the whole solution can be regarded as the result of an incident Kelvin wave of the form (4.4).

As an example, Fig. 1 shows a Kelvin wave of the form (4.4) where η_E is a Gaussian function of time. The wave is shown well before it is incident on the eastern boundary. The first two planetary waves reflected off the boundary are given by (4.5) with $n = 1$ and $n = 3$. These waves are shown in Fig. 2; this time well after they have been reflected. The planetary waves are foreshortened because they propagate at slower speeds, and their energy is concentrated farther from the equator than it is in the case of the Kelvin wave.

From the above, it follows that, if there is a region adjacent to the eastern boundary where the wind effect may be ignored, the velocity and sea-level anomalies over the whole region can be deduced from a single time series, namely that of η_E. This reconstruction has been done for the period 1971–73 using a table of monthly mean values of sea-level anomaly for Baltra running from June 1968 to March 1974, with linear interpolation used to make a continuous series. The anomalies for each month were found by subtracting the mean value for 1969–75 (January–May) or for 1968–75 (June–December). A missing value for March 1971 was filled with a value interpolated from the neighboring months. Fig. 3 shows the reconstructed surface anomaly field for October 1972 found in this way. The planetary waves, at any point, all originate at the eastern boundary some time before October 1972, so they are reconstructed on the basis of *past* data. The Kelvin wave, on the other hand, does not reach the eastern boundary until later, so its amplitude is reconstructed from *future* data. Since a Kelvin wave only takes 1½ months to propagate from the date line to the eastern boundary, it is only necessary to have values for the next two months for the reconstruction.

To give an idea of the effect of truncation at different levels, Fig. 3 compares results with two planetary waves (i.e., only coefficients up to q_4 retained), six planetary waves (i.e., only coefficients up to q_{12} retained) and with a large number of waves.

Values of η_E back to June 1968 have been used. Anomalies before that date affect only the high-n waves and are assumed to be zero. These high-n waves propagate so slowly that they may be severely affected by the mean flow, so there is no reason to believe that the solution with the large number of waves is any better than the solution with six waves. The solution involving only two planetary waves is useful near the equator away from the eastern boundary. It is not much use for $|y| > 3$ or for $x > -15$.

Longitude–time plots are shown in Fig. 4 so that

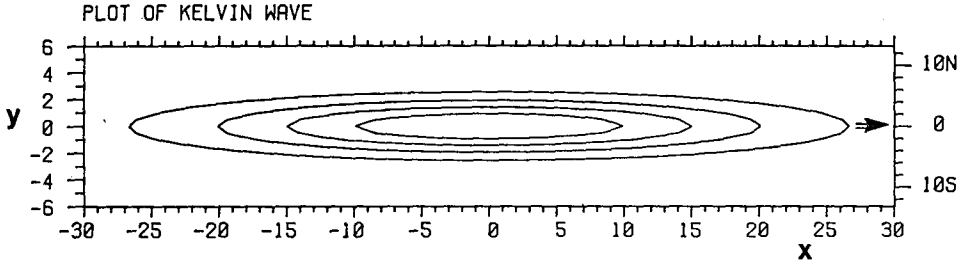

FIG. 1. Surface elevation contours for an eastward-propagating long Kelvin wave of unit amplitude with a Gaussian east–west profile. The contour interval is 0.2. Horizontal coordinates are given in nondimensional units. The scale at the right gives latitude assuming an equatorial Rossby radius of 2.2°. Note that the zonal current is proportional to the meridional gradient of sea-level, and is eastward for a wave of elevation.

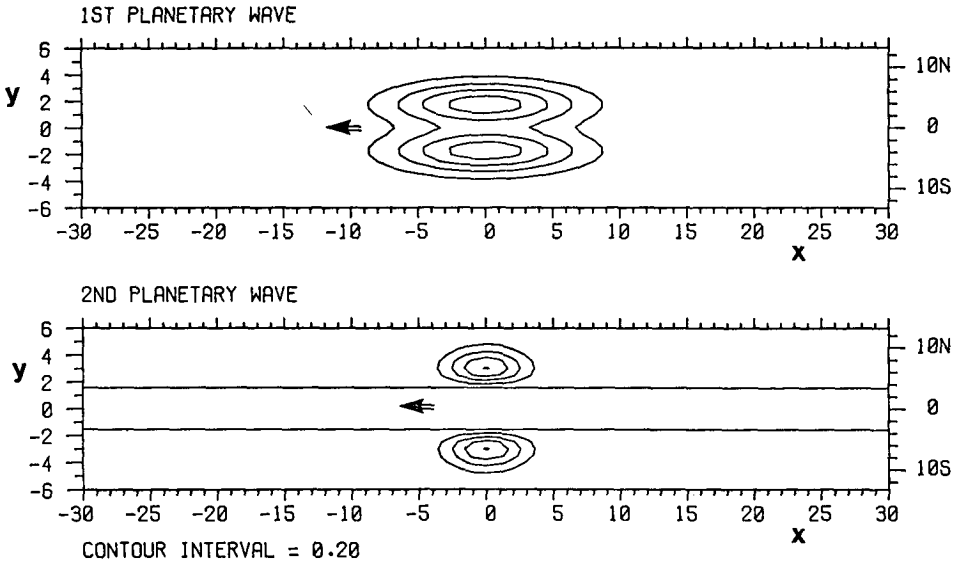

FIG. 2. Surface elevation contours for the first two planetary waves reflected from the Kelvin wave shown in Fig. 1. The first has one-third of the east–west scale of the Kelvin wave because it travels at one-third of the phase speed, and the second has one-seventh of the scale. The contour interval is again 0.2. Note that the zonal current is westwards for $|y| < 2$ for the first planetary wave of elevation, but eastward for $|y| > 2$.

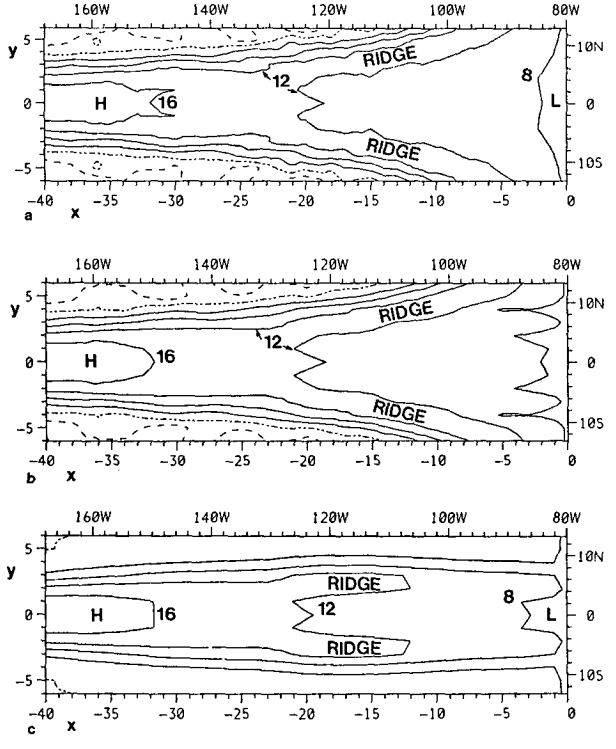

FIG. 3. (a) The sea-level anomaly for October 1972 computed without including wind effects. This is the "exact" solution obtained by adding contributions from more than 400 waves.

The remaining panels show effects of truncating the solution to include only (b) six and (c) two symmetric planetary waves. Both non-dimensional and dimensional horizontal scales are given. The contour interval is 4 cm. Positive contours are solid, the zero contour is dash-dot, and negative contours are dashed.

any propagation effects can be assessed. They show sea-level at (a) $y = -1.3$ (the latitude of Canton Island) and (b) $y = +0.9$ (the latitude of Christmas Island).

In practice, the wave amplitudes should be corrected by wind effects, but these will only become significant at some distance from the eastern boundary. Therefore the results shown in Figs. 3 and 4 should be as accurate as the model and the sea-level data will allow in the eastern part of the basin. The only way of assessing how far from the eastern boundary one can go before the wind corrections become significant is to calculate these effects and compare the reconstructions made with and without inclusion of wind effects. This is done in the next section.

5. Corrections for wind effects

In the last section, it was shown how all the wave amplitudes can be calculated from the sea-level η_E at the eastern boundary, and so used to reconstruct the entire sea-level and surface current field in the absence of any wind effect. In this section, it will be shown how the wind effect may easily be incorporated by integrating (3.4) and (3.6).

First, however, it is necessary to have appropriate surface wind stress data for the period of interest. For this purpose, a tape containing the Wyrtki–Meyers data (Wyrtki and Meyers, 1975, 1976) was used as a basis. This data is based on ship observations and gives monthly mean stress values in units of $m^2\ s^{-2}$ at anemometer height. Data are given for each 10° longitude band at latitude intervals of 2°. Unfortu-

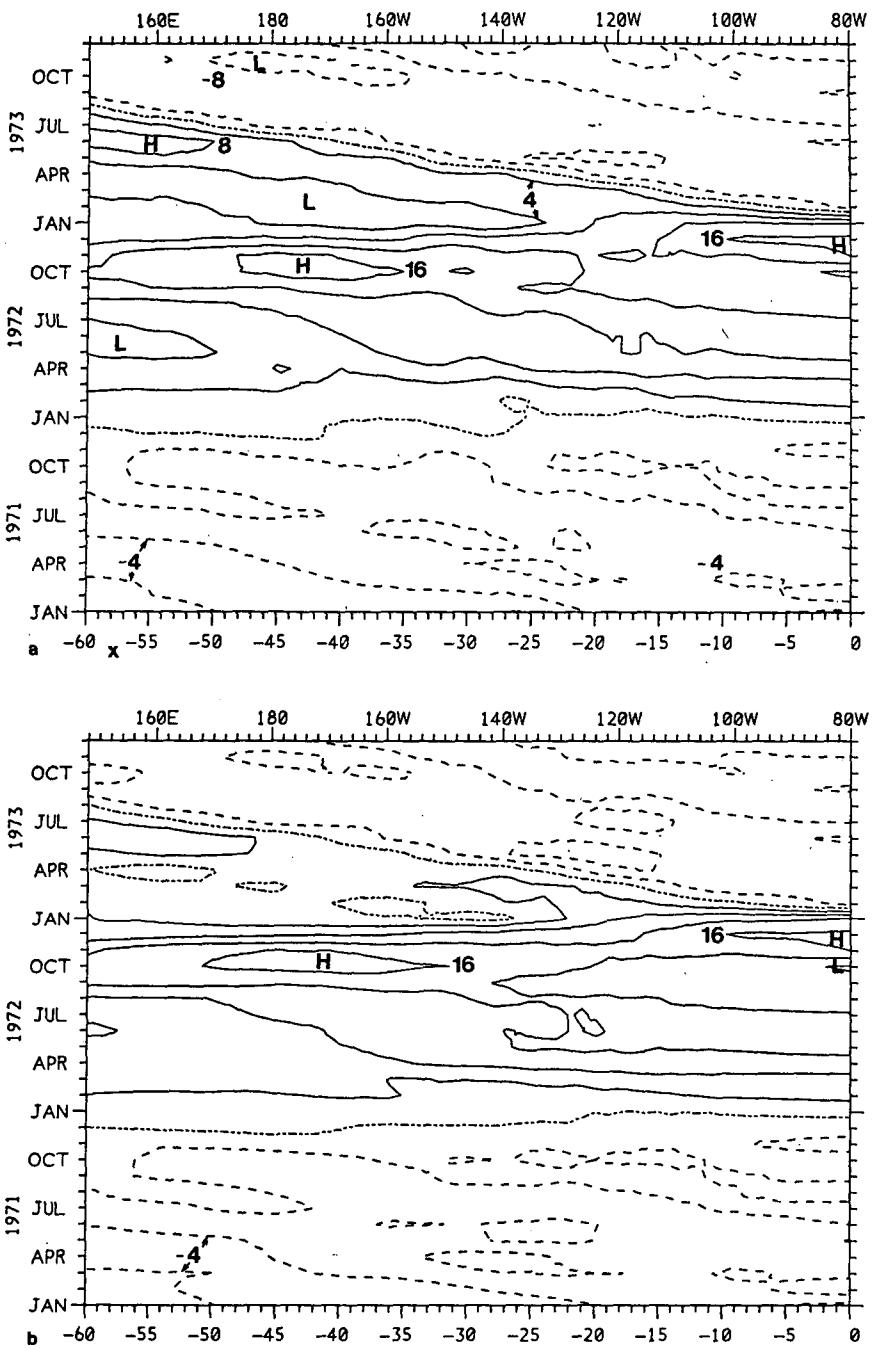

FIG. 4. Longitude–time plot showing contours of surface elevation anomaly at (a) $y = -1.3$, the latitude of Canton Island; and (b) $y = +0.9$, the latitude of Christmas Island. Wind effect is not included and 20 symmetric planetary waves are included in the computation. The contour interval is 4 cm. Positive contours are solid, the zero contour is dash-dot and negative contours are dashed.

nately, this data set ends in early 1973 and is rather sparse in the latter half of 1972. To extend the data set into 1973, the data from the atlas of Ramage *et al.* (1980) was obtained on magnetic tape. This covers the period November 1971 to December 1973, but only east of the date line. Also monthly mean surface wind, but not surface stress, is given. After some comparisons between monthly mean stress values and monthly mean wind (u, v) using the Wyrtki–Meyers data, it was decided to use the formula

$$\text{Eastward stress value} = 1.2u(u^2 + v^2)^{1/2}, \quad (5.1)$$

to give a value in $m^2 s^{-2}$ equivalent to those on the Wyrtki–Meyers magnetic tape. The stress in N m^{-2} is obtained from this value by multiplying by ρc_D (density by drag coefficient), which is assumed to have the value

$$\rho c_D = 0.0018 \text{ kg m}^{-3}. \quad (5.2)$$

The Ramage *et al.* data varies much more smoothly with time than the Wyrtki–Meyers data, presumably because it contains more information such as low-level winds derived from satellite pictures. Therefore, the Ramage *et al.* data was used where available, and the Wyrtki–Meyers data was smoothed by using 3-month running means (taking account of number of observations in each month) and this smoothed data was used for the region west of the date line and for the period before November 1971 at all longitudes. Anomalies for the merged data set were calculated by subtracting mean values for the period 1967–73.

Since the long-wave approximation is used, only the eastward component of the stress is required to calculate the forcing. At first, it was assumed that the stress has large scale, so an average value $\bar{X}$ of X between, say ±6°, could be used and the P_n forcing functions could be calculated from $\bar{X}$ using the relationships valid for a latitude-independent wind. However, it was found that when the ITCZ is near the equator, this assumption is not valid and P_2 may even have the opposite sign to the value calculated from $\bar{X}$. Thus the coefficients X_n in the series for X of the form (3.1) were calculated from a finite-difference version of the formula

$$X_n \int_{-\infty}^{\infty} D_n^2 dy = \int_{-\infty}^{\infty} X D_n dy, \quad (5.3)$$

which follows from the orthogonality relations (3.9). The coefficients follow from (3.6).

Next it was decided useful to fill in the few missing values west of the dateline in the second half of 1972 and in 1973. Dr. E. Rasmusson provided listings of $\bar{X}$ from which anomalies were calculated as above, and, in this case, X_n's were derived assuming the uniform-wind relationships with $\bar{X}$. These values were only inserted where no data was available from the other data sets. Where this data overlapped with the data set already compiled, detailed agreement was not very good. This was taken to indicate the data derived from the ship observations is rather noisy and certainly not reliable for an individual month or an individual 10°-longitude band. For larger time and space scales, the estimates of the surface stress are presumably meaningful, for otherwise the comparison made by Busalacchi and O'Brien (1981) between observed sea-level response and the results of a wind-driven model could not have been so good.

If no further smoothing was made, the results still looked very noisy, so a *spatial averaging* was performed by taking running means of 30° longitude. The results reported below are based on this smoothed data set. Because of the noise level in the original data, it is not assumed that a great deal of reliance can be placed on the results, but they at least might be expected to show the magnitudes and general features of the wind effects. Fig. 5 shows longitude time plots of the coefficients P_0 and P_1 calculated as described above. The negative values of P_0 in the west Pacific in 1971 correspond to strong easterlies (westward winds), and there is a strong easterly anomaly in the central Pacific at the end of the year. In 1972 the anomalies are mainly westerly (weak trades) in the west Pacific. The anomalies in 1973 are largely negative (easterlies) in both east and west. The patterns for P_2 and P_4 are broadly similar, but with signs reversed. The pattern for P_1 (Fig. 5b) is quite different, showing changes associated with north–south migrations of the ITCZ.

The wind effect was incorporated by recalculating q_0 to q_5 by adding wind correction terms to (4.4) and (4.5). These terms were obtained by integrating (3.4) and (3.6) between the eastern boundary and the point in question, the integration being in time for an observer traveling with the wave (Gill and Clarke, 1974). The integration in time used the trapezoidal rule with wind values for a given 10° longitude band being used for the time the wave was in that 10° band. The wind effect was ignored for coefficients q_n, $n > 5$. The results are shown in Fig. 6 in the same format as Fig. 4.

6. Evaluation of the sea-level results

The longitude-time curves for the latitudes of Canton Island and Christmas Island show only minor differences, and the general character of the anomalies, e.g., as seen by the sign changes, is the same whether or not the wind effect is included. Wave propagation stands out clearly at some times, e.g., when there is a period of rapid change. For instance, the Kelvin wave starting at the western edge around December 1972 can be seen propagating eastward to reach the eastern boundary by February 1973. The reflected planetary wave can then be seen moving westwards reaching the western boundary in August/September 1973.

In order to evaluate the results, Fig. 7 shows the comparison of predicted sea-level at Canton and Christmas Islands with observations. Results both with and without the wind correction are shown. The Christmas Island tide-gage record stopped in March 1972, and the Canton record began in May 1972, so they are non-overlapping. Since there are no disposable constants in the model, the level of agreement is encouraging. We consider the Christmas Island record first. The prediction with wind effect included is quite good with negative anomalies of approximately

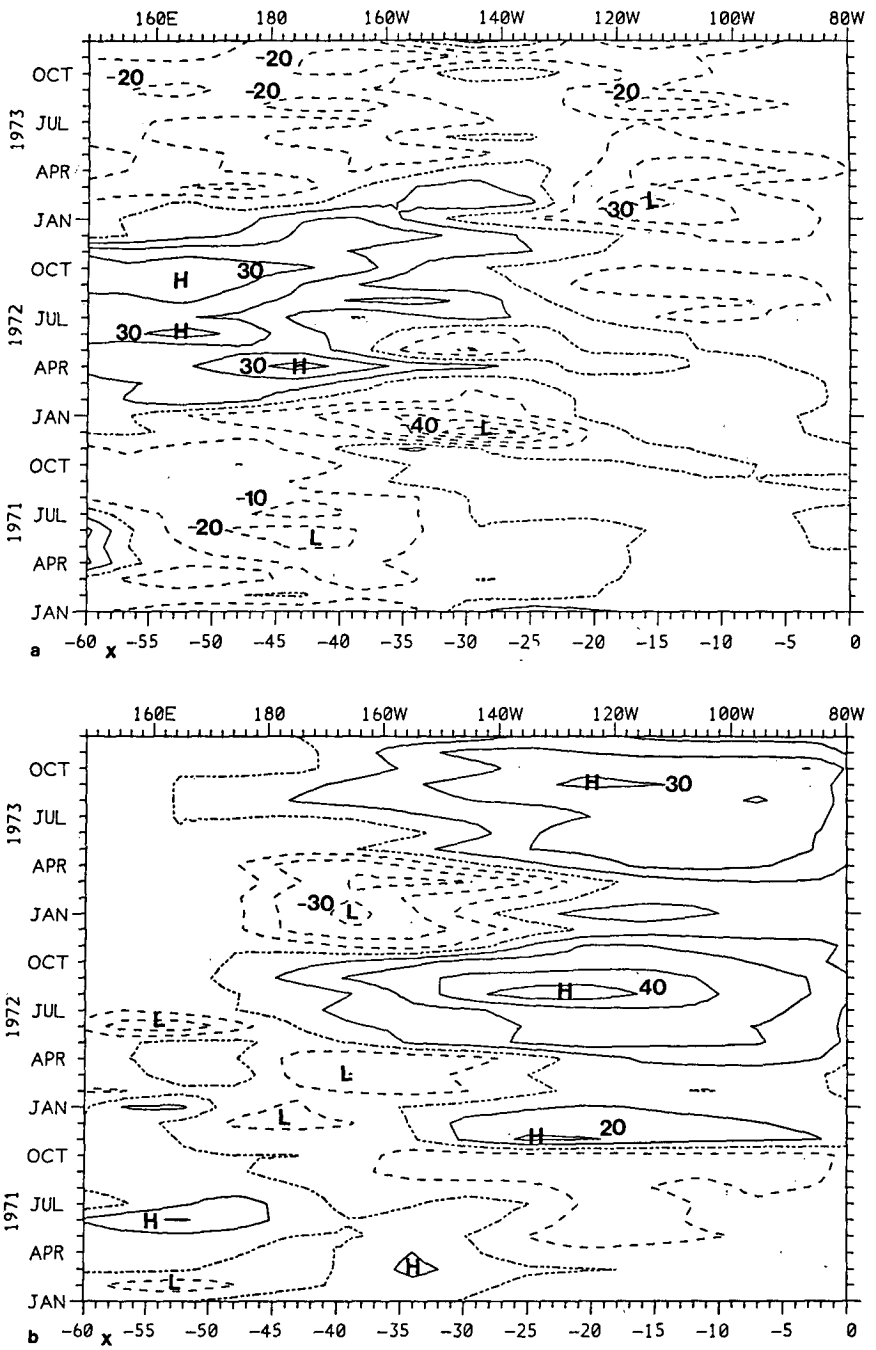

FIG. 5. Longitude-time plots of the coefficients (a) P_0 and (b) P_1 for the wind stress. The contour interval is 10 $m^2 s^{-2}$ which corresponds to ~0.018 N m^{-2}.

5 cm over most of 1971, and then a rapid change to positive values at the end of the year. According to the model, the Kelvin wave anomaly initiating the process changed to positive at Christmas Island in November 1971.

Next consider the Canton Island comparison. The most significant feature as far as the El Niño/Southern Oscillation phenomenon is concerned is the very large anomaly of 16 cm reached in October 1972. The magnitude of the peak is well predicted and the timing is also quite good. It can be seen that the large magnitude is due to the coincidence of a Kelvin wave peak, giving a contribution of 7 cm, and a planetary wave peak contributing another 10 cm. The planetary wave peak is due to the reflection of an earlier Kelvin wave peak which passed Canton Island in April 1972. The longitude-time plots show the phase coincidence is not so good farther west, so the peak gets smaller

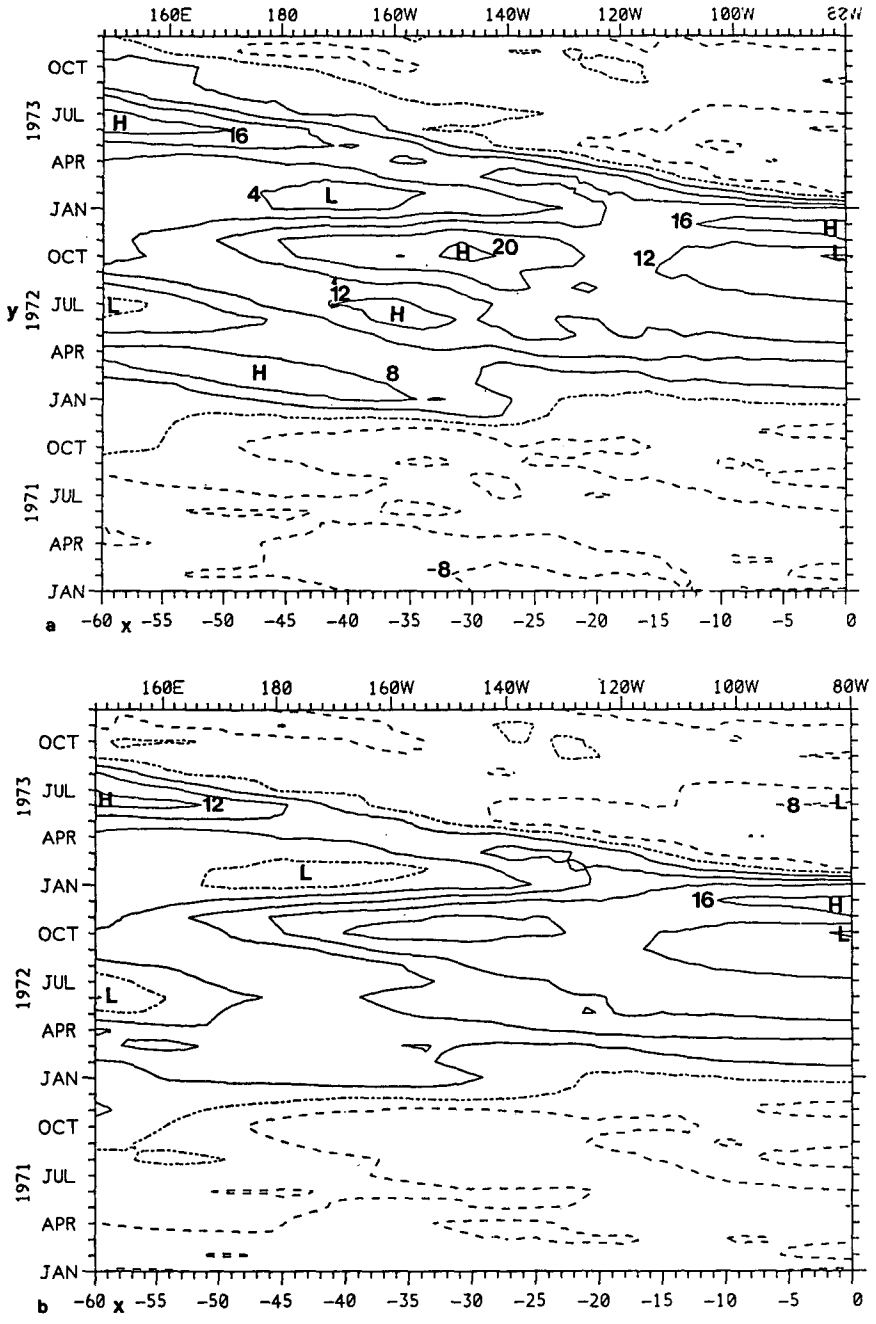

FIG. 6. As in Fig. 4, but with the wind effect included.

in that direction. Also, the anomaly is not so large near the eastern boundary. In other words, the very large sea-level anomaly is mainly found between 130°W and the date line.

The rapid drop in sea-level at Canton at the end of 1972 is also well-predicted, so the performance of the reconstruction technique is very good over 1971 and 1972. However, the performance in 1973 is not as good. The Kelvin wave which passed by Canton Island in October is reflected as a planetary wave giving another positive peak in May 1973 despite the Kelvin wave at that time giving a negative contribution. Also at this time, the trade winds have resumed and are stronger than normal, so building up the planetary wave even further. Thus, the calculation with wind effect included shows worse agreement than the calculation ignoring wind effects.

Although it is clear, e.g., from Gill (1982b), that nonlinear effects are important, particularly near the eastern boundary, it is surprising that the Canton Is-

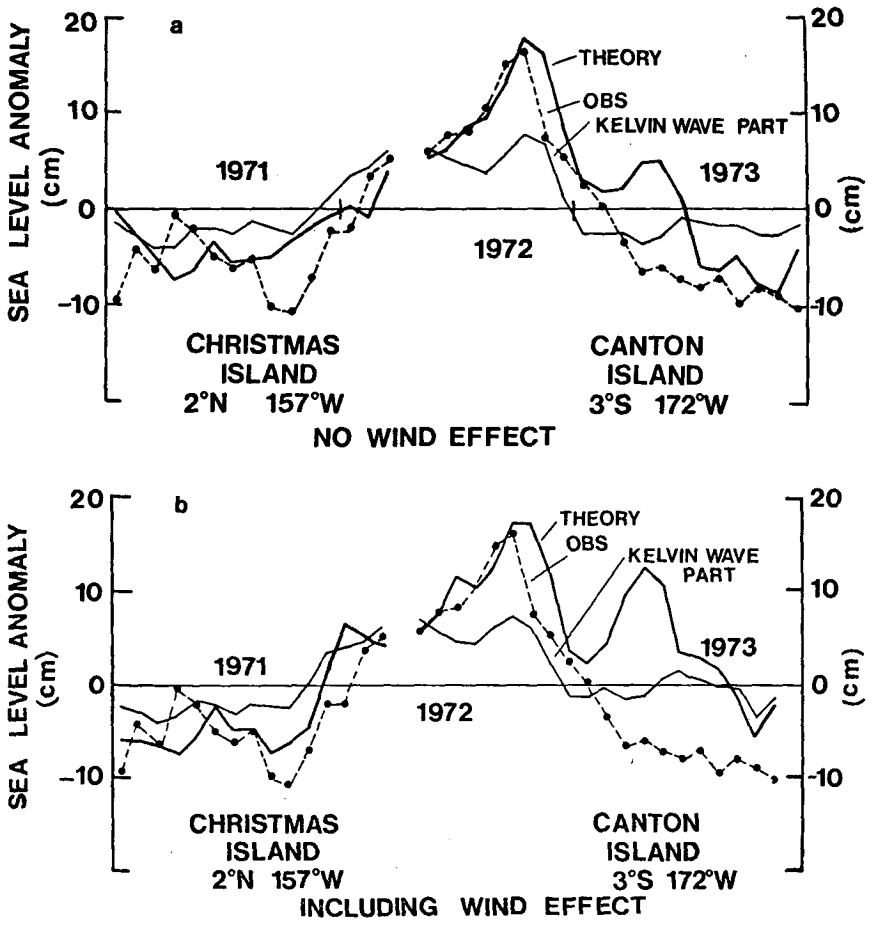

FIG. 7. A comparison of observed and computed sea-level anomalies at Christmas and Canton Islands. The thick solid line shows the result of the theoretical calculation, the Kelvin-wave contribution being shown by the thin solid line. The dashed line shows the observed anomaly. The results are (a) without wind effect and (b) including the wind effect. The Christmas Island record extends only to March 1972, while the Canton Island record begins in May 1972.

land record shows no evidence of the reflected planetary wave being present in May 1973. Clearly, there is still much to be learned about the behavior of waves in a realistic situation with features such as the shoaling of the thermocline toward the east included. Nevertheless, the results for the El Niño year, 1972, are very good and suggest that useful results will come from a study of the current anomalies during the year. Until now, ideas about the behavior of currents during El Niño events have been somewhat speculative, so using the long-wave reconstruction method to calculate magnitudes and distributions of anomalous currents appears to be a major step forward.

Before discussing currents, it is useful to point out some simple approximations for calculating sea-levels and currents near the equator. For this approximation, wind effects are ignored because the results shown in Figs. 4 and 6 are similar. Secondly, all but the Kelvin wave and first planetary wave are ignored. Fig. 3 shows this is reasonable for points close to the equator and not too near the eastern boundary. Then (4.4), (4.5), (3.17) and (3.22) give

$$\eta = 2^{-1/2}\{D_0(y)\eta_E(t - x) + [D_0(y) + \tfrac{1}{2}D_2(y)]\eta_E(t + 3x)\}. \quad (6.1)$$

Averaging over the range $|y| < 2$ and denoting the average by an overbar, the values obtained are

$$2^{-1/2}\bar{D}_0 = 0.53, \quad 2^{-1/2}\bar{D}_2 = 0.01, \quad (6.2)$$

which will be approximated by ½ and zero respectively, then (6.1) gives

$$\bar{\eta}(t, x) = \tfrac{1}{2}[\eta_E(t - x) + \eta_E(t + 3x)]. \quad (6.3)$$

This form has a certain appeal in that it is exactly correct at the eastern boundary $x = 0$.

Applied to the value of $\bar{\eta}$ at the longitude of Canton Island, it means taking the Galapagos sea-level anomaly time series η_E shown in Fig. 8a, and averaging it

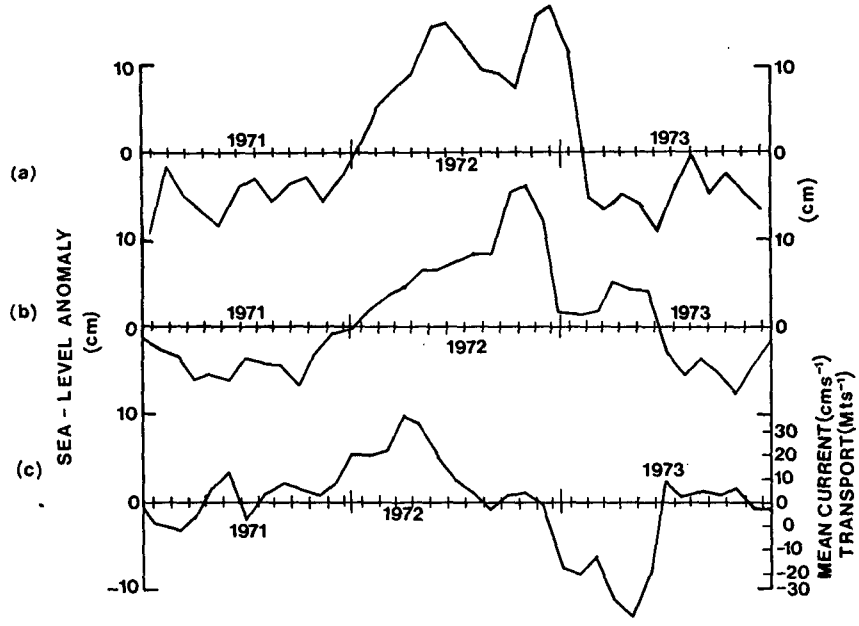

FIG. 8. (a) The time series of the sea-level anomaly η_E at Baltra, Galapagos Islands, used to generate the solutions shown in this study. (b) Curve obtained by adding $\frac{1}{2}\eta_E$, 1½ months earlier than (a), to $\frac{1}{2}\eta_E$ 4½ months later. This gives an approximation to $\bar{\eta}$, the mean sea level for $|y| < 2$ at the longitude of Canton Island. (c) Curve obtained by subtracting $\frac{1}{2}\eta_E$ 4½ months later than in (a), from $\frac{1}{2}\eta_E$ 1½ months before (a). This gives an approximation to $g^{-1}c\bar{u}$, where $\bar{u}$ is the mean current for $|y| < 2$ at the longitude of Canton Island.

with the same time series displaced by six months. Here $\bar{\eta}$ is, in fact, the average of η_E one and a half months later, and η_E four and a half months before the given time. Fig. 8b shows this average and it gives a reasonable approximation to the observed sea-level anomaly series for Canton or Christmas Island.

Returning now to the full calculation with many waves and including the wind effect, Fig. 9 shows the sea-level anomaly pattern at three-monthly intervals as reconstructed by the method described earlier. In October 1971, the anomaly field is mainly negative and a negative planetary wave can be seen near the date line. Three months later, a positive Kelvin wave can be seen giving a maximum elevation on the equator near Canton Island. During the remainder of the year, the area of positive anomaly steadily increases. The very large anomaly in October 1972 is evident, this being due to the coincidence of positive Kelvin wave and positive planetary wave. The pattern is qualitatively similar to that of the observed thermocline depth anomaly shown in Fig. 11 of Gill (1982b). In January, 1973 the effect of the negative Kelvin wave is evident in the western part with a strong wave front between 140 and 110°W.

7. Temperature anomalies on the equator in the central Pacific

In the previous sections a technique is established for obtaining estimates of surface current anomalies in the equatorial Pacific. There are no direct measurements of currents against which to evaluate these estimates, but the method does appear to have some skill in estimating sea-level changes. In the absence of any other information, these results will now be used to estimate advective effects on the heat balance of the surface layers. They indicate that advection by the surface current is a dominating effect near the equator, and the fact that the changes due to this effect have the observed amplitude and phase supports the idea that the estimates are meaningful. This section discusses the central Pacific. The situation is different near the eastern boundary, and this will be discussed in the following section. Finally, there is a discussion in Section 9 of the heat budget for the surface layer spanning the whole region from the date line to the American Coast and from ~6½°N to 6½°S.

We now consider the central Pacific where temperature anomalies tend to be concentrated in an equatorial strip. According to long-wave theory, the currents which might advect the temperature field are zonal to a first approximation. Therefore it is the zonal current which will be evaluated. For simplicity, attention is concentrated on the average zonal current anomaly $\bar{u}$, over the range of latitudes $|y| < 2$, i.e., between ~4½°N and 4½°S. The result (with wind effects included) for $\bar{u}(x, t)$ is displayed in a longitude-time plot in Fig. 10. The most impressive feature is the band of positive values starting in late 1971 and

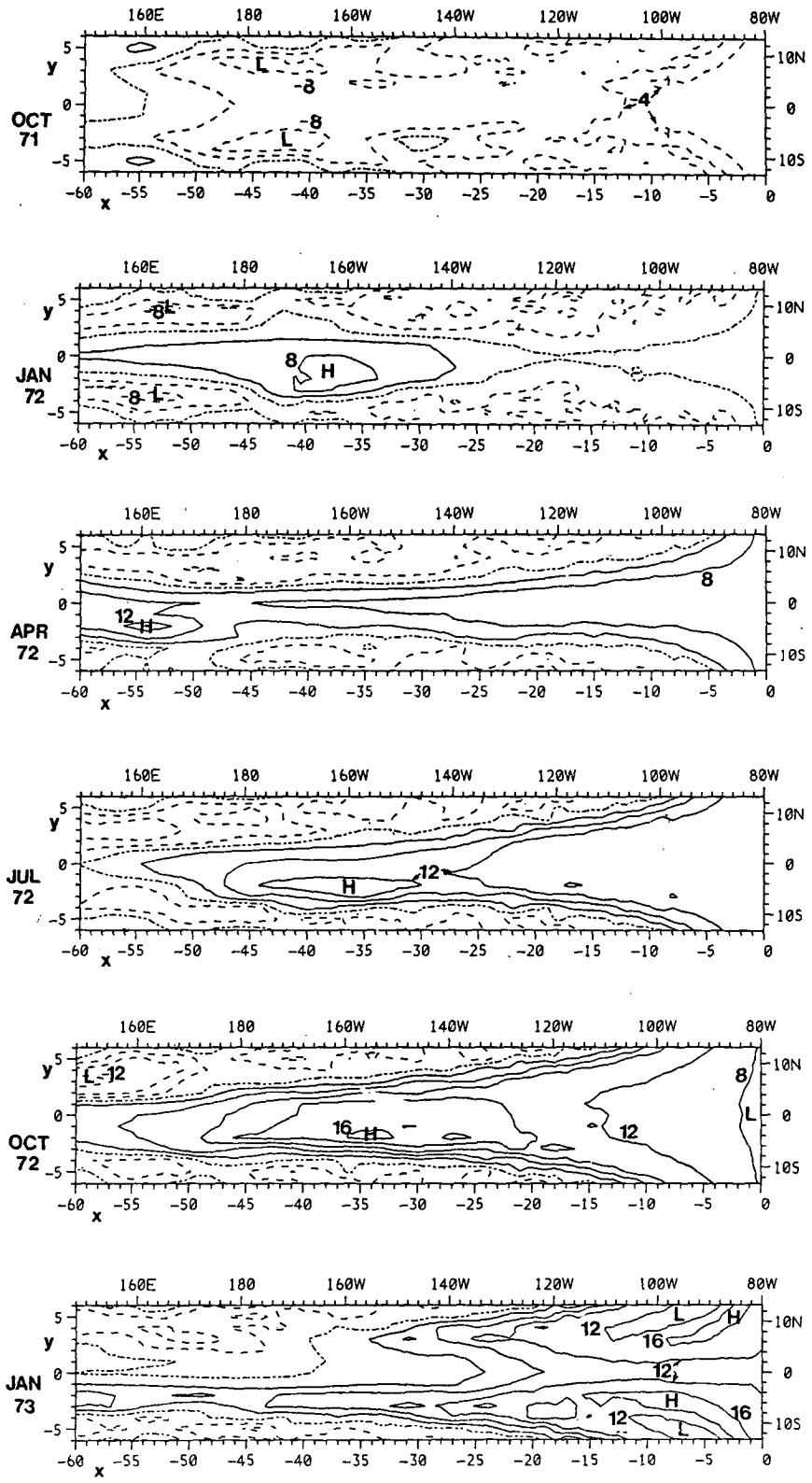

FIG. 9. Estimated sea-level anomaly fields at three-month intervals for October 1971 to January 1973. Positive contours are shown solid, the zero contour dash-dot and negative contours dashed. The contour interval is 4 cm. Both nondimensional and dimensional horizontal scales are given.

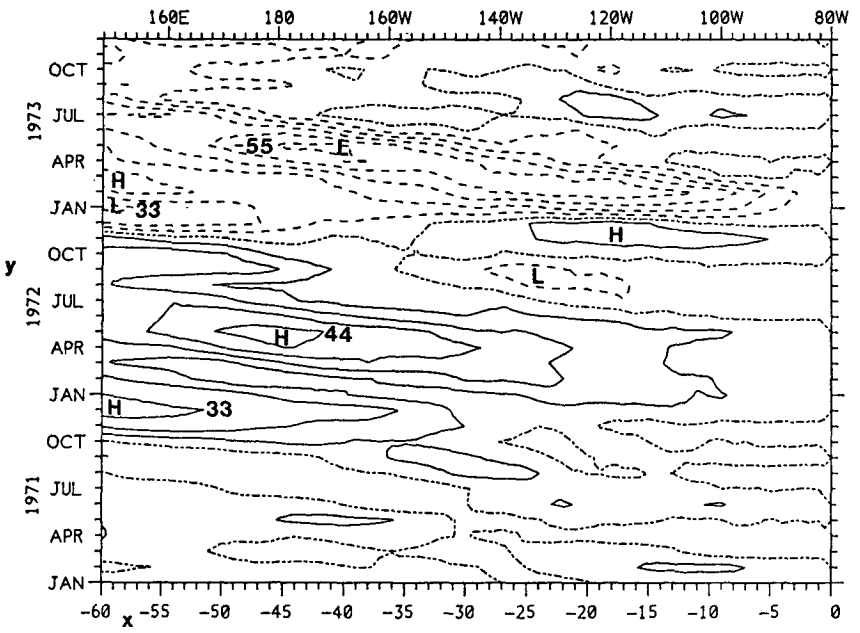

FIG. 10. Longitude-time plot showing contours of mean current anomaly, the mean being for $|y| < 2$. The contour interval is 0.04 non-dimensional units, i.e., ~ 11 cm s^{-1}. The calculation includes the wind effect.

continuing until late 1972. In other words, there is an anomalous eastward motion in the central Pacific for an entire year. This deduction is generally consistent with that obtained by Wyrtki (1977, Fig. 8) using sea-level differences between islands to estimate changes in currents.

One immediately asks how far water particles are transported by this anomalous motion. A calculation of particle displacements every $\frac{1}{16}$ of a month was made, using interpolated values at the start position each time. The results are shown in Fig. 11. This shows that the anomalous displacements are large,

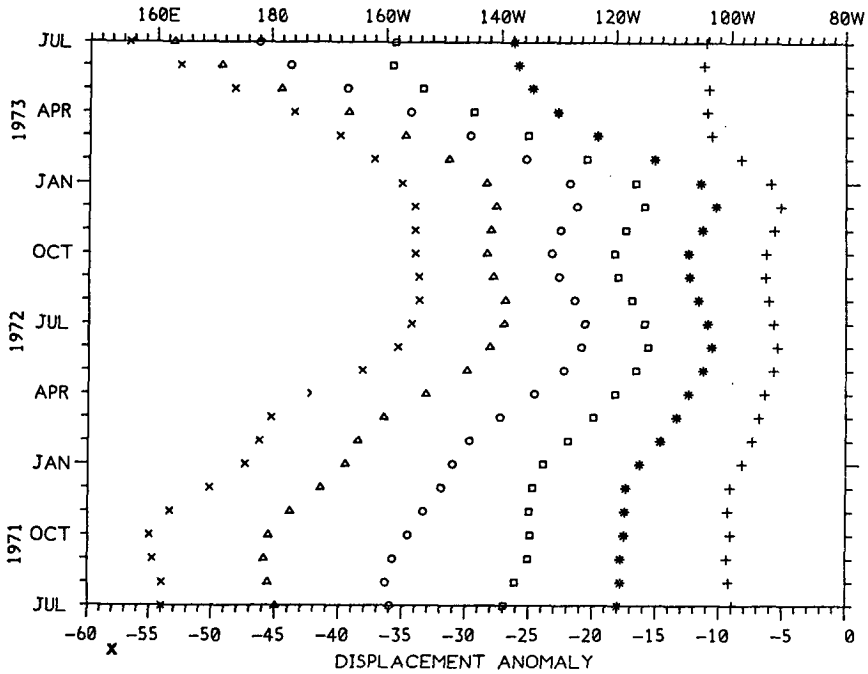

FIG. 11. Zonal particle displacements as functions of time for hypothetical particles moved by the current field displayed in Fig. 10.

i.e., about one-third of the way across the ocean from their initial position. In particular, a particle starting at 160°E in the latter half of 1971 would find itself at 160°W a year later. (This is the motion relative to the normal mean plus seasonal motion, i.e., the anomalous motion.) Furthermore, this is the mean over $|y| < 2$; excursions by the mean over $|y| < 1$ would be even greater. The idea that large eastward displacement anomalies occur during El Niño events is consistent with the estimates made by Wyrtki (1979) for the 1976 event. His estimates were based on the change in volume of the warm upper waters of the west Pacific.

It is now possible to make an assessment of the causes of the temperature anomalies observed. Consider the terms which can contribute to temperature anomalies in the mixed layer. The terms which occur in linear theory are:

1) Advection of mean temperature by anomalous currents,
2) Advection of temperature anomaly by mean currents,
3) Anomalous heating through the surface,
4) Anomalous non-advective transfer of heat through the base of the thermocline.

The last term involves diffusive effects which probably depend on such quantities as the shear between the surface current and the undercurrent. Since the model does not predict significant changes in this, the fourth effect will be ignored. There are also nonlinear effects such as advection of temperature anomalies by current anomalies, but these will largely be ignored as well, leaving the discussion to the first three effects.

What creates the central Pacific anomaly? Only terms 1 and 3 can create anomalies, so which is the more important? Fig. 12 gives the results of an attempt to assess term 3. It is based on results for the net heat input into the ocean in the rectangle 180–160°W, 6¼°S–6¼°N as given in the El Niño atlas of Ramage *et al.* (1980). The best that could be done with such a short record was to take the two-year period November 1971 to October 1973 and regard the anomaly for a particular month as the departure from the mean value for that month over the two years. The results in Fig. 12 show the anomalous heat content obtained by integrating the anomalous heat input in time. If the anomaly is spread over a 100 m mixed layer, the result shows a maximum positive anomaly of 0.4°C at the end of May 1982 and very weak anomalies for the latter half of 1972. In fact, the observed anomalies are quite different, as Fig. 12b shows. This is calculated from the El Niño atlas data in the same way as the heat-flux anomaly. Thus effect 3 cannot be responsible for the anomalies.

Now consider the first effect. The mean temperature is greater in the west than the east, so the greatest positive temperature anomalies occur when the anomalous displacement (shown in Fig. 11) has its maximum value eastwards. Fig. 11 shows this occurs over the latter half of 1972, precisely when the temperature anomaly is greatest. Furthermore, the magnitudes are approximately right. Westward of 160°E, surface temperatures in September–November are normally in the range 29.5–30°C (Robinson, 1976).

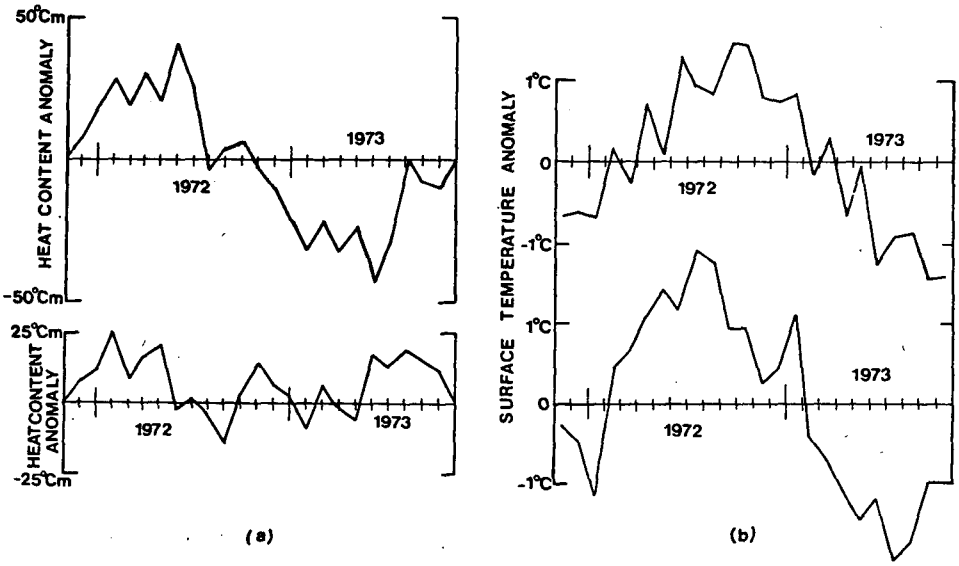

FIG. 12. (a) Heat content anomalies computed from the data in the atlas of Ramage *et al.* (1980). The upper panel is for the region 180–160°W, 6¼°N to 6¼°S. The lower panel is an average for the data points nearest to the eastern boundary between 5 and 20°S at intervals of 2½° of latitude. Anomalies are relative to the two-year mean. The scale is in degrees times meters. (b) Surface temperature anomalies computed in the same way.

If a particle is moved to 160°E, as suggested by Fig. 11, where temperatures are normally 26.5–27.5°C, the temperature will be ~3°C above normal. The El Niño atlas indeed shows temperatures of 29½°C in the latter half of 1972, as opposed to values of ~27°C during the following year (see also Gill 1982b, Fig. 8).

Similarly, a particle originating at 160°W would have, according to Fig. 11, a displacement anomaly which would move it to 130°W. This also corresponds to a temperature anomaly of ~3°C and is consistent with observations. Since the first effect can explain the observations so well and effect 3 cannot, it is concluded that temperature anomalies in the central Pacific are mainly caused by anomalous zonal advection.

It should be pointed out that anomalous vertical advection does not contribute according to the theory, as this merely causes movements of the thermocline without changing the mixed-layer temperature significantly.

It should also be noted that the anomalous eastward advection that causes the temperature anomaly starts late in 1971. The largest current anomalies are in the first half of 1972 and are of order 20–30 cm s^{-1}, and correspond to transport anomalies over the first 100 m of order 20–30 megaton s^{-1} (Sv). These values result from a coincidence of the positive Kelvin wave associated with the first peak at Baltra and a negative planetary wave which is the reflection of the negative Kelvin wave which was present at Baltra in late 1971. Both these waves give positive contributions to the mean current in the region $|y| < 2$. The positive contribution from the Kelvin wave is clear from Fig. 1 because sea-level decreases away from the equator for a positive Kelvin wave. Fig. 2 shows that, in the region $|y| < 2$, sea-level also decreases away from the equator for a *negative* first planetary wave. This is brought out clearly if the approximation corresponding to (6.3) is applied to the current. The result is

$$g^{-1}c\bar{u}(t, x) = \tfrac{1}{2}[\eta_E(t - x) - \eta_E(t + 3x)], \quad (7.1)$$

and this curve is shown in Fig. 8c. The timing of initiation of the displacement anomaly fits in well with the timing of the beginning of the positive temperature anomaly. Rasmusson and Carpenter (1982, Fig. 22) find this begins around the change of the year for the composite anomaly at all latitudes east of 160°E, but is a couple of months earlier near the date line.

It is also important to note that the explanation of temperature anomalies in terms of anomalous advection applies only to the strip within ~5° of the equator, whereas Rasmusson and Carpenter (1982) show the anomalies spread over ~15°. A possible explanation of this is that once anomalies are created, advection of temperature anomalies by the mean flow become significant. Thus the mean Ekman flux away from the equator will tend to spread anomalies over a greater range of latitudes.

Finally, Fig. 12 shows that the greatest rate of cooling occurs in the second half of 1972, when the temperature anomaly is greatest, as may be expected. Thus the cooling is a response to the anomaly created by the anomalous advection rather than a cause of the anomaly.

8. Temperature anomalies near the eastern boundary

The anomalous changes become somewhat different in character near the eastern boundary where: 1) the zonal flow vanishes; 2) seasonal changes are large (Horel, 1982); and 3) changes in sub-surface structure are observed (Gill, 1982b) to be quite different from the central Pacific in that the thermocline is spread out a great deal rather than just being displaced vertically. We consider, in particular, the coastal strip between the equator and 20°S. Fig. 12 shows the anomalous heat exchange for this strip according to the atlas of Ramage *et al.* (1980) and also shows the observed temperature anomaly according to the same data. If the heat input anomaly is assumed to be distributed over a mixed layer depth of 30 m, the bottom panel of Fig. 12a shows a maximum temperature of 0.8°C reached early in 1972 and removed again by the middle of the year. By contrast, the observed anomaly reaches a maximum of nearly 2°C during mid-1972 and is positive for the whole year. Again, it is clear that the anomaly is not caused by anomalous heat exchange with the atmosphere.

Now consider the anomalous advection along the coastal strip itself. There are two components to this; first, horizontal advection parallel to the coast, and second, vertical motion. Eq. (2.15), in the absence of wind, shows that the anomalous poleward displacement along the coast is in phase with the sea-level. There is some evidence to support this (Gill, 1982b), but perhaps with displacement lagging a little. The magnitude of the displacement y is given by integrating the dimensional form of (2.15), namely,

$$\frac{1}{y}\frac{dy}{dt} = \frac{1}{H_e}\frac{d\eta_E}{dt}, \quad \text{that is,} \quad \ln\left(\frac{y}{y_0}\right) = \frac{\eta_E}{H_e}, \quad (8.1)$$

where y_0 is the initial particle position and H_e the equivalent depth. In Gill (1982b), it was shown that η_E/H_e was observed to be O(1), the appropriate H_e being that of the second baroclinic mode. This would move a surface particle initially at 4°S, e.g., to 11°S, and be sufficient to give a temperature anomaly O(2°C) [using the mean annual temperatures given by Horel (1982)]. Clearly, linear theory is being overstretched, therefore, not very much reliance can be placed in this result, but a possible order of magnitude is indicated.

The vertical spreading of the thermocline (Gill, 1982b, Fig. 5) is observed to be in phase with the sea-

level changes along the boundary, and this produces a large subsurface temperature anomaly. This anomaly can be rapidly transferred into the surface layer by the mean upwelling which appears to continue (Brink *et al.*, 1980) unabated throughout El Niño conditions. Thus, the coastal surface temperature anomaly, whether due to anomalous horizontal advection or to upwelling, is approximately in phase with sea-level as observed. The magnitude of the surface temperature anomaly that might be expected from the upwelling mechanism would be a little less than that of the subsurface anomaly. This is also O(2°C) (Gill, 1982b, Fig. 6). Thus, both horizontal advection and upwelling can contribute to give temperature anomalies of the right magnitude and with the appropriate phase.

Effects of the coastal anomaly are spread downstream by the mean surface current which Wyrtki (1965) shows is equatorward along the coast, and then westward in the South Equatorial Current, which has its largest velocities near the equator. The normal seasonal picture is consistent with the following idea: The upwelled water along the coast becomes increasingly cold from March to September, according to the normal Southern Hemisphere pattern. This cold water is advected into the South Equatorial Current and along the equator creating a cold tongue spreading westwards from the eastern boundary. The effect is clearly seen in the longitude time plot of Horel (1982, Fig. 6b) and extends to ~140°W. The rate of westward spreading is of order 20° per month or 1 m s^{-1}. The northern boundary of the tongue forms the Galapagos front, which becomes very strong by September, and the pattern is similar to the one found in a numerical model by Philander and Pacanowski (1981). In this model, upwelling was only produced in the Southern Hemisphere because the wind was uniformly northward, producing cold water along the coast only in the Southern Hemisphere. Mean advection spread this cold water along the equator forming a cold tongue similar to the observed one.

To illustrate the development of the cold tongue, Fig. 13 shows successive positions of the 21 and 26°C isotherms between March and September 1972 in comparison with normal years. Also shown are positions of hypothetical fluid particles moved according to the Wyrtki (1965) surface current charts, which suggest, but by no means prove, that advection is an important process in establishing the tongue. Clearly, the tongue is very poorly developed in 1972, and this can be attributed to two factors: 1) the relative warmth of the source water for the tongue, i.e., the upwelled water at the coast; and 2) the slackening of the south equatorial current during the El Niño year indicated by calculations discussed in Section 7.

It is perhaps appropriate here to comment on phase relationships between the eastern and central Pacific. Hickey (1975) and Rasmusson and Carpenter (1982) have drawn attention to the apparent westward prop-

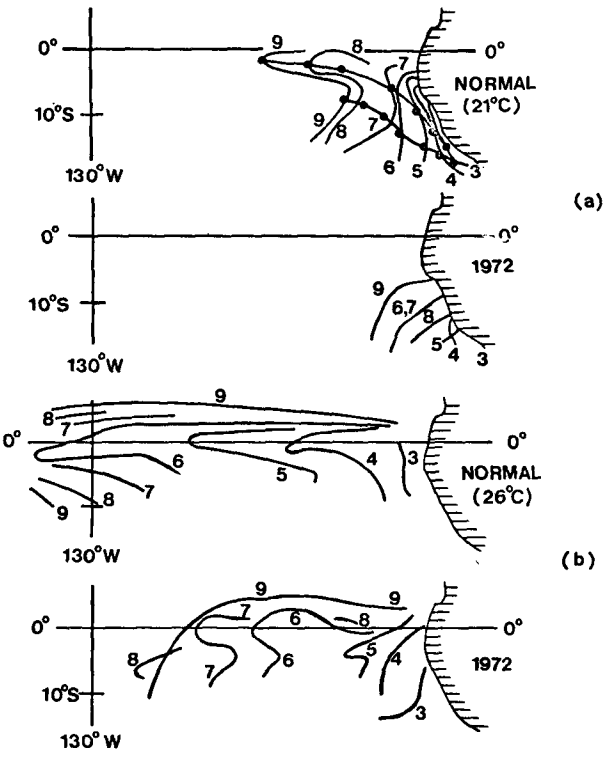

FIG. 13. Successive monthly positions of (a) the 21° isotherm and (b) the 26° isotherm for March to September of normal years compared to 1972. Months are numbered 3 (March) to 9 (September). The first panel also shows successive positions of particles moved by the mean surface currents given by Wyrtki (1965).

agation of surface temperature anomaly. The present work indicates that the explanation is not simply that one is following a wave. The clearest picture of how such a phase difference can be created comes from Fig. 8 where the method of construction is particularly simple. The peak in sea level at Canton Island follows the first peak at the eastern boundary by several months, but the explanation depends on the double-peaked structure of the incoming wave and on interference between the incoming and reflected waves. To be specific, the Canton Island peak is due to constructive interference between the second peak Kelvin wave and the reflection from the first peak.

9. Heat content anomalies for the equatorial strip

The calculation in Section 7 leads to the conclusion that there is a massive flux of surface water and therefore heat from the west Pacific to the east during an El Niño year, so it is of interest to find the flux values given by the present calculation. The transport anomaly across the date line was calculated for the latitude range $|y| < 3$ (i.e., between 6½°N and 6½°S) since $y = \pm 3$ is approximately the point where the current anomaly changes sign (i.e., sea-level anomaly is stationary). Changes with time have a similar pattern to those shown in Fig. 10, but magnitudes are larger

(transports are 20% larger but average currents are 20% smaller). The anomaly was positive (eastwards) for the 12 months beginning October 1971 and averaged 26 Sv over the mixed layer (which occupies the top 100 m) for the year. The average current over the cross section is 18 cm s^{-1}.

Now consider the implications of this huge water movement for the mass and heat balances for the volume bounded meridionally by $y = \pm 3$ (i.e., latitudes 6½°N and 6½°S), bounded zonally by the date line and the American coast, and bounded vertically by the surface and the 100 m depth level. The anomalous zonal mass flux into this volume across the date line in the 12-month period is sufficient to displace half the volume defined above. Some of the displaced water (~55%) is lost by downward motion across the 100 m level, the remainder is lost by poleward displacement across the bounding latitudes. The proportion involved in downward rather than poleward displacement was estimated from the model results.

The amount of heat involved in the mass exchanges through the volume depends on the average temperature difference between the warm water involved in the inflow anomaly across the date line and the cold water involved in the outflow anomaly across the bottom and sides of the volume. This temperature difference is approximately 5°C, estimated on the basis of Robinson's (1976) atlas and taking into account the way the outflow is divided between the bottom and the sides. The average anomalous influx of heat into the volume by advection then works out at half a petawatt (5×10^{14} W) which, in the absence of other effects, would raise the average temperature of the volume by 2½°C. If all the heat were lost to the atmosphere instead, the average anomalous heat flux to the atmosphere across the surface would be 31 W m^{-2}. These figures are, of course, very approximate because they are based on a crude model, but they give a good idea of the orders of magnitudes involved.

Another element of the heat balance for this same equatorial volume is the flux across the surface. The time variation of this flux, as calculated from the atlas of Ramage *et al.* (1980), is shown in the second panel of Fig. 14. Also shown is the evaporation contribution to this flux and the averages of the surface temperature and zonal wind for the same area. The heat flux shows quite large variations despite being averaged over such a large area. Consider first the year from 1 November 1971 to 31 October 1972 nearest to the year for which the anomalous advection was calculated (it is one month later). The average surface temperature in this period warms up by 2.6°C but the heat flux is little different from that of the following 12 months, corresponding to a slight relative gain of 0.06 petawatts. This is consistent with the idea that the warming is mainly due to anomalous advection, and the magnitude of the warming is consistent with the above calculation. In other words, the data from

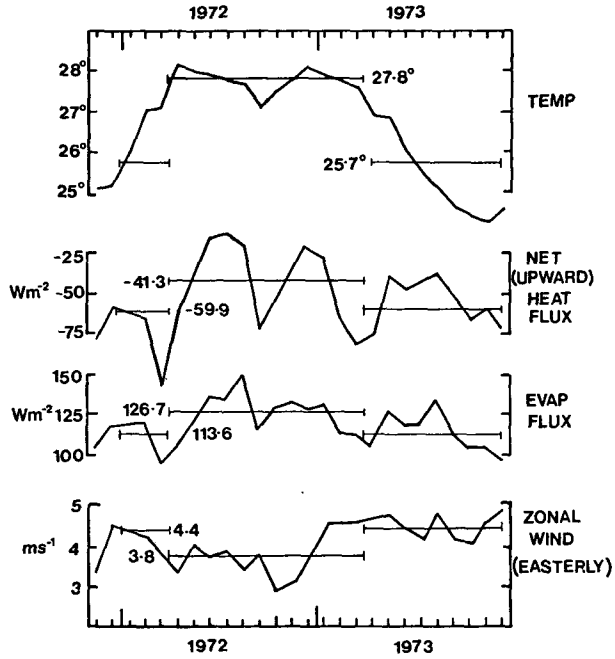

FIG. 14. Average of (a) surface temperature, (b) net upward surface heat flux, (c) surface evaporative flux and (d) surface zonal wind for the equatorial strip between the date line and the South American coast, and between 6¼°N and 6¼°S. Data is from the atlas of Ramage *et al.* (1980). Also shown are averages for the warm years starting 1 April 1972 and a control year comprising the three months before and the nine months after the warm year.

the Ramage atlas shows there was little heat input across the surface between 1 November 1971 and 31 October 1972, so the surface temperature increase of 2.6°C must be due to other factors. The previous calculation indicates the primary factor responsible for the increase was anomalous advection of warm water into the volume from the west.

It is interesting now to look at the data presented in Fig. 14 from another point of view, namely the relation between surface temperature anomaly and heat loss anomaly. The year with the highest temperatures was the one commencing 1 April 1972, i.e., displaced about six months from the year of anomalous heat input (which is by advection), as one would expect. This warm year can be compared with a control year comprising January to March 1972 and April to December 1973 (see also Ramage and Hori, 1981). The surface temperature in the warm year averaged 2.1°C higher than in the control year, and the heat loss is 0.3 petawatts higher (an average flux of 19 W m^{-2}). The interpretation of this result is that about half the heat gained by anomalous advection is lost six months later by heat loss to the atmosphere. Thus, as Fig. 11 indicates, if there is anomalous eastward advection between October 1972 and September 1973 which is of the same magnitude as the westward advection the year before, the ocean will not return to its original state but will be colder because

of the anomalous heat loss to the atmosphere. Another interpretation of the heat loss figure is that, if applied to the top 100 m of the equatorial surface layer, it would correspond to a cooling rate of 1.5°C per year. If this rate is proportional to temperature anomaly, and has this value when the anomaly is 2.1°C, then the *e*-folding time for temperature anomalies to be removed would be 1.4 years. In other words, if there is a surface temperature anomaly and no oceanic processes to maintain it, the atmosphere will remove the anomaly fairly quickly.

The data given in Fig. 14 has another interesting feature. It might be argued that if the tropical ocean becomes warmer than normal, it will lose heat mainly by evaporation. Fig. 14 shows that although this is true, only 13 W m^{-2} of the 19 W m^{-2} net flux anomaly is due to evaporation. The other 6 W m^{-2} involves changes in the radiative balance. Furthermore, the evaporative flux does not depend on the temperature as one might expect. If one assumed that the relative humidity and wind speed were fixed, and that the air–sea temperature difference were zero, then the evaporative flux would increase in proportion with the saturation specific humidity. A 2.1°C increase in temperature gives a 16% increase in this quantity, whereas the observed increase in evaporative flux is 11%. The *mean* zonal wind is actually 15% below normal in the warm year—enough to cancel out the effect due to increased saturation humidity. Thus it does not seem possible to construct simple rules about how heat flux changes relate to surface temperature changes.

10. Discussion

The warming of surface waters in the equatorial Pacific during El Niño years is due to a massive anomalous flux of warm surface water from west to east over a period of about one-year duration. In the central Pacific, the timing and magnitude of the temperature anomaly can be explained on the basis of anomalous horizontal advection. This creates the anomaly in a strip extending about 6° either side of the equator, and the mean Ekman flux in the surface layer can spread the anomaly over a wider range of latitudes. Similarly, an anomaly can be produced on the eastern boundary by anomalous poleward advection, and then spread laterally by the mean Ekman flux in the surface layers. In this region, mean upwelling can also transfer subsurface anomalies (associated with the thickened thermocline) into the surface layer and these can be spread along the equator by horizontal advection.

The calculations in the present paper are based on a very simple model. Presumably, more accurate estimates could be made with better models which could include such effects as nonlinearity, the horizontal structure of the mean field, seasonal changes, and a better representation of vertical structure. However, with more sophisticated models it is harder to make use of the information available in sea-level observations, as was done here.

The model used in this paper turned out to be quite successful in explaining surface temperature anomalies as being due to anomalous currents. But what

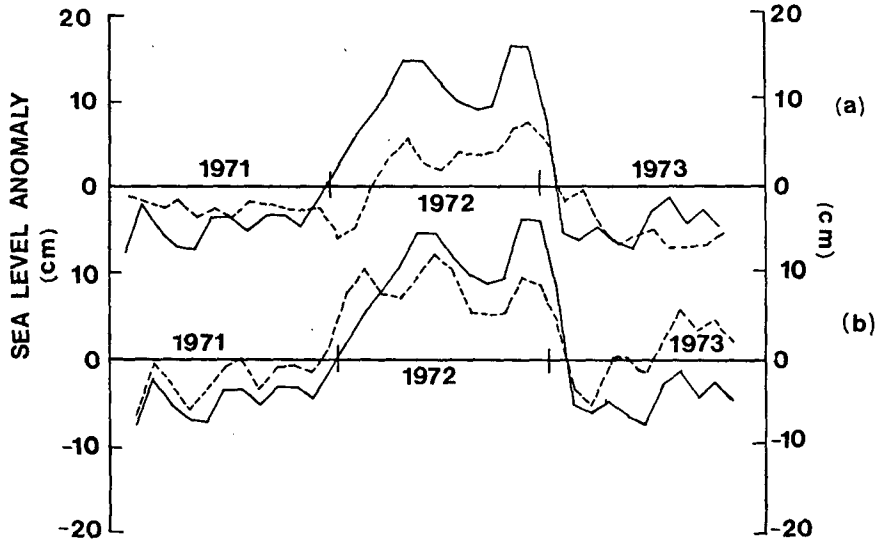

FIG. 15. (a) Observed sea-level anomaly η_E at the eastern boundary (solid line) compared with the anomaly (dashed line) estimated from the wind effect between $x = -60$ and $x = 0$ (i.e., assuming a Kelvin wave starting from $x = -60$ with zero amplitude). (b) Estimated amplitude of the Kelvin wave at the western boundary $x = -60$ without (solid line) and with (dashed line) the wind effect included. Values have been multiplied by $2^{1/2}$ and phase shifted two months so the solid curve is the same as in (a). The second curve in (a) is then equal to the difference between the two curves in (b).

causes the anomalous currents? Presumably, a wind-driven numerical model would be capable of tracing the cause to features of the wind-stress anomaly field. The reconstruction technique used in this paper leads to a different approach to the question of cause. This technique emphasizes the role of Kelvin waves incident on the eastern boundary. Thus, the natural question to ask in this context is "What determines the amplitude of the Kelvin-wave anomaly at the eastern boundary?" In the reconstruction technique, there is a contribution to this amplitude due to the wind anomaly effects accumulated during the passage of the wave from west to east across the Pacific. The remainder must be attributed to the Kelvin wave having non-zero amplitude at the western boundary, i.e., to emission of Kelvin waves from the western boundary, or alternatively to errors in the data or shortcomings in the model. There are many reasons to have reservations about the wind stress data and about the model, yet it is of interest to see what results the model gives. This information is given in Fig. 15, and presented in two different ways.

First, Fig. 15a shows the magnitude the Kelvin wave would have at the eastern boundary if it had zero amplitude at the western boundary and was produced solely by the winds shown in Fig. 4. The interesting feature of this diagram is that there is good correlation between the calculated and observed waves, but the "predicted" positive sea-level anomaly is less than half the observed, and starts two or three months late. The differences in magnitude make one question if the wind effect is underestimated for some reason, *e.g.*, filling data gaps in wind data using climatology inevitably reduces the magnitude of anomalies, or more than one mode may contribute to the effect.

Another way of displaying the same information is shown in Fig. 15b. The solid curve is the same as in Fig. 15a, but is now interpreted as the amplitude of the Kelvin wave at the western boundary when calculated without accounting for wind effect. The dashed curve shows the result of the calculation with the wind effect included. (Both curves are phase shifted by the propagation time across the ocean so as to be aligned with Fig. 15a.) The dashed curve would correspond to small magnitudes if the wind effect were mainly responsible for the observed amplitude at the eastern boundary. However, the values with wind effect are quite substantial—only ~30% smaller than the values without. In other words, the conclusion from this data set and model, if taken at face value, is that Kelvin waves are emitted from the western boundary with significant amplitude. In particular, the initiation of the positive anomaly, according to this model, is mainly due to an emitted Kelvin wave, rather than a wind event generating a Kelvin wave directly. Note also that the wind effect (the dashed curve in Fig. 15a) only begins to give a positive contribution to the Kelvin wave in March 1972, after the warm patch has been initiated. It might be speculated that this is due to a positive feedback in which the winds respond to the warming in such a way as to amplify the Kelvin wave.

Hopefully, observations will improve sufficiently so that Kelvin waves can be measured at several longitudes, the strength of the wave emitted from the western boundary can be directly observed, and the evolution of the wave in crossing the Pacific can also be followed. Also, one would hope that wind data will become good enough for accurate estimates of the wind effect on the Kelvin-wave amplitude to be made so that comparisons can be made with observation. Furthermore, one hopes to be able to make measurements of the westward-propagating planetary waves and thereby learn something about their evolution and about the reflection process at the eastern boundary.

Acknowledgment. I would like to thank Jeffrey Blundell for the programming work and for the computer-drawn diagrams.

REFERENCES

Abramowitz, M., and I. A. Stegun, 1964: *Handbook of Mathematical Functions.* Nat. Bur. Stnds., Washington, DC.

Brink, K. H., D. Halpern and R. L. Smith, 1980: Circulation in the Peruvian upwelling system near 15°S. *J. Geophys. Res.*, **85**, 4036–4048.

Busalacchi, A. J., and J. J. O'Brien, 1981: Interannual variability of the equatorial Pacific in the 1960's. *J. Geophys. Res.*, **86**, 10 901–10 907.

Cane, M. A., 1979: The response of an equatorial ocean to simple wind stress patterns. *J. Mar. Res.*, **37**, 233–252.

——, and E. S. Sarachik, 1981: The response of a linear baroclinic equatorial ocean to periodic forcing. *J. Mar. Res.*, **39**, 651–693.

Erdelyi, A. W., W. Magnus, O. Oberhettinger and F. G. Tricomi, 1953: *Higher Transcendental Functions,* Vol. II. McGraw Hill, 396 pp.

Gill, A. E., 1975: Models of equatorial currents. *Numerical Models of Ocean Circulation,* Nat. Acad. Sci., Washington, DC, 181–203.

——, 1982a: *Atmosphere-Ocean Dynamics.* Academic Press, 662 pp.

——, 1982b: Changes in thermal structure of the equatorial Pacific during the 1972 El Niño as revealed by bathythermograph observations. *J. Phys. Oceanogr.*, **12**, 1373–1387.

——, and A. J. Clarke, 1974: Wind-induced upwelling, coastal currents and sea-level changes. *Deep-Sea Res.*, **21**, 325–345.

Hickey, B., 1975: The relationship between fluctuations in sea-level, wind stress and sea-surface temperature in the equatorial Pacific. *J. Phys. Oceanogr.*, **5**, 460–475.

Horel, J. D., 1982: The annual cycle in the tropical Pacific atmosphere and ocean. *Mon. Wea. Rev.*, **110**, 1863–1878.

Hurlburt, H. E., J. C. Kindle and J. J. O'Brien, 1976: A numerical simulation of the onset of El Niño. *J. Phys. Oceanogr.*, **6**, 621–631.

McCreary, J., 1976: Eastern tropical ocean response to changing wind systems: with application to El Niño. *J. Phys. Oceanogr.*, **6**, 632–645.

Philander, S. G. H., and R. C. Pacanowski, 1981: The oceanic

response to cross-equatorial winds (with application to coastal upwelling in low latitudes). *Tellus,* **33,** 201–240.

Ramage, C. S., and A. M. Hori, 1981: Meteorological aspects of El Niño. *Mon. Wea. Rev.,* **109,** 1827–1835.

——, C. W. Adams, A. M. Hori, B. J. Kilonsky and J. C. Sadler, 1980: *Meteorological Atlas of the 1972–73 El Niño.* UHMET 80-03, Dept. Meteor., University of Hawaii, 101 pp.

Rasmusson, E. M., and T. H. Carpenter, 1982: Variations in tropical sea-surface temperature and surface wind fields associated with the Southern Oscillation/El Niño. *Mon. Wea. Rev.,* **110,** 354–384.

Robinson, M. K., 1976: Atlas of North Pacific Ocean *Monthly Mean Temperature and Mean Salinities of the Surface Layer.* NOO-RP-2, U.S. Navy, 19 pp., 173 figs.

Wunsch, C., and A. E. Gill, 1976: Observations of equatorially-trapped waves in Pacific sea-level variations. *Deep-Sea Res.,* **23,** 371–390.

Wyrtki, K., 1965: Surface currents of the eastern tropical Pacific Ocean. *Inter-Amer. Trop. Tuna Comm. Bull.,* **9,** 280–304.

——, 1975: El Niño—The dynamic response of the equatorial Pacific Ocean to atmospheric forcing. *J. Phys. Oceanogr.,* **5,** 572–584.

——, 1977: Sea level during the 1972 El Niño. *J. Phys. Oceanogr.,* **7,** 779–787.

——, 1979: The response of sea surface topography to the 1976 El Niño. *J. Phys. Oceanogr.,* **9,** 1223–1231.

——, and G. Meyers, 1975: The trade wind field over the Pacific Ocean. Rep. HIG-75-1, Hawaii Inst. Geophys., 25 pp., 25 figs.

——, and ——, 1976: The trade wind field over the Pacific Ocean. *J. Appl. Meteor.,* **15,** 698–704.